An implicit algorithm with fast convergence for evolution of a preexisting-closed plane-strain hydraulic fracture

KAIRUI LI[1,2], N. N. SMIRNOV[1,3*], CHENGZHI QI[4], A. B. KISELEV[1], MINGYANG WANG[2]
[1]Faculty of Mechanics and Mathematics, Lomonosov Moscow State University, Leninskie Gory 1, Moscow,119991, RUSSIA
[2]State Key Laboratory for Explosion & Impact and Disaster Prevention & Mitigation, Faculty of Defense Engineering, Army Engineering University of PLA, Nanjing, 210007, CHINA
[3] Scientific Research Institute for System Analysis of the Russian Academy of Sciences, Nakhimovskiy str. 36-1, Moscow,117218, RUSSIA
[4] Beijing High Institution Research Center for Engineering Structure and New Material, Beijing University of Civil Engineering and Architecture, Beijing, 100044, CHINA
*mech.math.msu@inbox.ru

Abstract: - This paper is focused on the evolution from the initial opening to the initial propagation of a preexisting-closed plane-strain hydraulic fracture. An implicit finite difference algorithm is proposed for avoiding solving this solid-liquid coupling nonlinear problem composed by lubrication equation for fluid flow and elasticity equation for fracture opening. By accurately estimating the main unknowns of the problem at each time step: estimating the length of fluid-zone by transient velocity of fluid front, the length of lag-zone by zero opening at the fracture tip, and the fracture opening at the next time step by the fluid volume conservation, the convergence velocity is deeply improved. In order to improve model accuracy, an adaptive time step method is adopted because of gradually decreasing velocity of fluid front. The relationship between grid length and time step is discussed for balancing convergence velocity and good accuracy, and a balance threshold determining scales of grid length and time step is given. Based on the improved implicit algorithm the evolution laws of the first stage from the initial opening to the complete opening and the second stage from complete opening to initial propagation are obtained.

Key-Words: - Preexisting-closed plain-strain hydraulic fracture; Implicit algorithm; Adaptive time step

1 Introduction

Hydraulic fracturing today as a technique is widely applied in the exploitation of petroleum and natural gas. Nevertheless, evolution of fluid pressure, fracture opening and fracture geometry in hydraulic fracture is a very complex mechanical problem, related to the nonlinear coupling of fluid and solid mechanics: on one hand, the lubrication equation governs flow of hydraulic fluid in fracture [1], which is a nonlinear partial differential equation of fracture opening and fluid pressure obtained by combining continuity equation and Poiseuille law; on the other hand, the elasticity equation provides a relationship between the net pressure (fluid pressure minus far-field stress) and formation deformation [2]. More complicated is that the two equations are calculated not in the same region of hydraulic fracture with a fluid lag: lubrication equation is only used in the fluid-zone, but elasticity equation presents the solution of fracture opening, which consists of two terms: one term is the contribution of net pressure in fluid-zone and the other is the contribution of net pressure in lag-zone. Furthermore, because of complex integral form, this solution can't be directly substituted into the lubrication equation. In addition, in this mechanical problem there are two fronts that need to be determined: the fluid front and the fracture front, which are respectively determined by the global continuity equation of fluid in an integral form along the whole fluid-zone and the boundary conditions of fracture opening at fracture tip [3,4]. Only if locations of the two fronts are known, can calculation intervals of the above two governing equations be determined, and then solutions of this problem can be found. If the seepage of hydraulic fluid, inhomogeneity and anisotropy of formation are taken into account, this mechanical problem will be more difficult to be modeled and solved.

At present, with the development of numerical computation, there are many complex and sophisticated numerical methods for simulating hydraulic fracturing evolution, including finite element method (FED) [5-8], finite-discrete element method (FDEM) [9], finite volume method (FVM) [10], displacement discontinuity method (DDM)

[11,12], which can consider many influence factors in models with the help of computer's high-speed computing ability. But in these papers many problems, for example, how numerical methods work, how these methods iteratively converge, or whether there are any methods or measures to accelerate convergence, are not given in details. In fact, these researches don't focus on the quality of numerical methods, but only on the final numerical results. In these numerical methods two-dimensional mesh [5-10] and traditional elasticity theory are used to obtain the whole stress and strain fields, which greatly increase the amount of calculation and slowly converge due to the large grid number. It is worth noting that Garagash, Detournay and Lecampion [13-16] have performed a lot of deep researches on the numerical algorithm for plain-strain hydraulic fracture by considering different influence factors. Based on scaling and dimensionless formulation, they obtained similarity solutions and asymptotic solutions at the early time and the large time (a finite lag and zero lag, respectively), and then analysed the composition of solutions and added the higher order terms to obtain the solution at the intermediate time. The complete solution consists of the combined solutions at the early, the intermediate and the large time. They also gave a detailed explanation for discretizing the nonlinear partial differential lubrication equation and the elasticity equation.

But the introduction of high order terms and the transform of elasticity equation into semi-analytical polynomial form for solving the complex integral make the final solution more cumbersome and complicated, not conducive to numerical calculation. In addition, in their algorithms grid number is very few, and most grids are concentrated near the fracture tip for calculating stress intensity factor, which will lead to large errors for fluid-zone. Other problem of these algorithms is the slow convergence with an average 60 iterations per time step in paper [17], the algorithm of which is widely used in many papers [13-16] for calculating the propagation of plain-strain hydraulic fracture. In most papers [5-16] they didn't analyse and evaluate the numerical algorithm and didn't study improving the convergence velocity. It is generally known that quality of iterative algorithm is also an important criterion for evaluating a model. So in this paper we will describe and evaluate in detail a fast convergence algorithm aimed at calculating the evolution process of a preexisting-closed plain-strain hydraulic fracture. And this algorithm with fast convergence can also be used in the stage of hydraulic fracture propagation.

This paper is organized as follows. The mathematical model of a preexisting-closed plain-strain hydraulic fracture is presented in Section 2 followed by model discretization in Section 3. The model discretization is the core idea for calculation, it determines which discrete method will be used in the model. Section 4 describes the detailed iterative algorithm and methods to quickly find the accurate numerical solution for improving convergence velocity. The numerical evolution results and analysis of algorithm quality are given in Section 5. Section 6 follows with some conclusions.

2 Mathematical Model

We consider a two-dimensional plane-strain hydraulic fracture with a small half-length l_0 under completely closed state in an infinite elastic medium characterized by Young's modulus E, Poisson's ratio ν and fracture toughness K_{Ic}. Because of the symmetry of the problem with respect to the injection point at $x=0$ only one fracture wing is shown in Fig. 1 (a). After the injection of hydraulic fluid into the initially closed fracture, two surfaces of fracture start to open under internal fluid pressure $p_f(x,t)$ and far-field normal stress σ_0 perpendicular to fracture surfaces. As fluid injection continues, the proportion of opened fracture becomes larger and larger, see Fig. 1 (b), with l_f being the length of fluid-zone, l_{op} being the length of opened fracture equal to the sum of fluid-zone length and lag-zone length. When the tip of opened fracture coincides with the tip of initial fracture, fracture is completely opened ($l_{op}=l_0$), and if stress field at some moment satisfies the fracture propagation condition, the initial fracture will propagate forward. This paper mainly describes the phase from the initial open of closed fracture until its initial propagation, which is a very short process obtained by Pauya [18]. So formation's permeability is neglected.

2.1 Elasticity equation

According to the Linear Elastic Fracture Mechanics (LEFM) in infinite elastic and homogeneous medium within a fracture, relationship between the net pressure and fracture opening w was formulated in an integral form by Sneddon [3]:

$$\frac{E\pi}{4(1-\nu^2)}w(x,t)=\int_0^{l_f}p(\zeta,t)G(x,\zeta)d\zeta+\int_{l_f}^{l_{op}}p'(\zeta,t)G(x,\zeta)d\zeta,\quad 0\le x\le l_{op} \tag{1}$$

where $p(\zeta,t)=p_f(\zeta,t)-\sigma_0$, $p'(\zeta,t)=p_{lag}(\zeta,t)-\sigma_0$ are net pressures in fluid-zone and lag-zone at moment t, respectively. $p_{lag}(x,t)$ is the pressure of lag-zone. The first and the second integrals on the right side of equation (1) are contributions of net pressure in fluid-zone and net pressure in lag-zone, respectively. The integral kernel G is defined as

$$G(x,\zeta)=\ln\left|\frac{\sqrt{l_{op}^{\ 2}-x^2}+\sqrt{l_{op}^{\ 2}-\zeta^2}}{\sqrt{l_{op}^{\ 2}-x^2}-\sqrt{l_{op}^{\ 2}-\zeta^2}}\right|. \tag{2}$$

2.2 Lubrication equation

The flow of a viscous incompressible Newtonian fluid in the fluid-zone ($0<x<l_f$) is determined by lubrication equation and continuity equation [1]

$$\frac{\partial w}{\partial t}+\frac{\partial q}{\partial x}=0,\quad q=-\frac{w^3}{12\mu}\frac{\partial p}{\partial x}, \tag{3}$$

where q denotes the fluid flow rate per unit width of the fracture, and μ is fluid viscosity. Combining the two equations, the nonlinear differential equation is obtained

$$\frac{\partial w}{\partial t}=\frac{1}{12\mu}\frac{\partial}{\partial x}\left(w^3\frac{\partial p}{\partial x}\right). \tag{4}$$

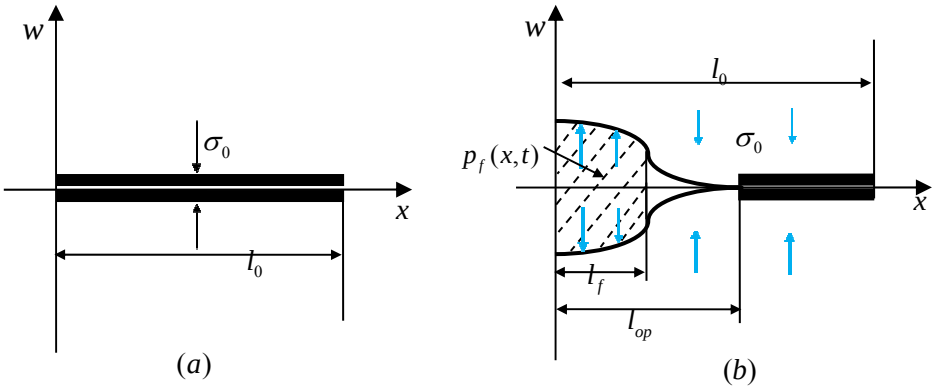

Fig. 1 Profiles of the initial hydraulic fracture: (a) Completely closed state of the initial fracture. (b) Partially opened state of the initial fracture at some moment.

2.3 Boundary conditions

The boundary condition at the injection point is expressed as constant injection rate:

$$q=\frac{Q_0}{2}=-\frac{w_0^3}{12\mu}\frac{dp}{dx},\quad x=0 \tag{5}$$

where w_0 is the fracture opening at $x=0$, and Q_0 the total well injection rate. According to pressure continuity along the whole fracture, the boundary condition at the fluid front is

$$p_f=p_{lag},\quad x=l_f \tag{6}$$

where $p_{lag}(x,t)$ is decided by many factors (formation permeability, pore fluid in formation and so on). Here we make use of the assumption of a zero pressure in the lag-zone as in the paper [16]

$$p_{lag}=0,\quad l_f\le x\le l_{op}. \tag{7}$$

The boundary condition at fracture tip in the phase of fracture propagation is determined by the propagation criterion: stress intensity factor K_I equals formation toughness K_{Ic} [19,20]. But for the preexisting fracture the upper and lower surfaces are not connected together, as shown in Fig. 1(a), so this fracture propagation criterion is not suitable for fracture open. Here we replace it with another boundary condition, namely, the smooth fracture closure condition, which was first proposed by Zheltov and Khristianovic [21], proved by Barenblatt [4] in mobile equilibrium process of fracture propagation and later applied in KGD model [22]. Because fracture surfaces are subjected to the interior fluid pressure and the far-field stress and are not adhered to each other, at the tip of lag-zone (the end of the opened fracture) the two surfaces are needed to be close smoothly,

$$\frac{\partial w}{\partial x}=0, \quad w=0, \quad x=l_{op}. \tag{8}$$

According to the volume conservation of an incompressible fluid, another important condition is written as

$$\int_0^{l_f} w dx=\frac{Q_0 t}{2}, \tag{9}$$

the main role of this condition is to determine the location of fluid front l_f .

2.4 Initial conditions

The real initial conditions at $t=0$: l_f=0, w=0 and the known l_0 (see Fig. 1(a)) are singular for solving the governing equations of the model. To avoid this problem we choose a moment t_0 (t_0 is unknown and very close to 0) as the relative initial time. Because at this small moment t_0 inlet pressure at the well P_0 is much great (P_0 □ $\sigma_0>0$) and the initial length of fluid-zone l_f^0 is very small (l_f^0 □ l_0), so the fluid pressure distribution can be assumed as linear [6]:

$$\begin{aligned} p_f(x,t)&=P_0\left(1-\frac{x}{l_f^0}\right), \quad 0\le x\le l_f^0 \\ p_{lag}(x,t)&=0, \qquad\qquad l_f^0<x\le l_{op}^0 \end{aligned} \tag{10}$$

where l_{op}^0 represents the length of opened fracture at this moment t_0 . It is emphasized that the quasi-linear pressure distribution of fluid-zone at the very early time is obtained by Garagash [15]. It means that the assumptation of linear pressure distribution as the relative initial condition is reasonable.

3 Method of Solution

The whole model is governed by equations (1) and (3) with conditions (5) – (10), which is a nonlinear differential equation system. Because of the complex integral form in equation (1) about w and p , anyone of the two unknown variables in equation (3) cannot be substituted by the other. So we can only solve the two equations separately and make the solutions from equations (1) and (3) approximate each other by iteration.

3.1 Fracture discretization

The studied phase from initial open of the closed fracture until its initial propagation can be further divided into two stage: the first stage is from the initial open to complete open. In this stage fluid front and front of the opened fracture move forward with different velocities until $l_{op}=l_0$; the second stage is from fracture complete open to initial propagation, in which only fluid front moves forward, the front position of the opened fracture keeps still. In the first stage we use a uniform moving mesh along the whole opened fracture, including fluid-zone and lag-zone, see Fig. 2(a). Δx is the grid length, m and n are node numbers in fluid-zone and lag-zone at some moment t_k , respectively. Actually, the total node number is $m+n-1$ because of the last point in fluid-zone coinciding with the first point in lag-zone. v_f and v_{op} denote velocities of fluid front and front of the opened fracture. As the fluid front and the front of opened fracture move forward, grid numbers of the two zones increase.

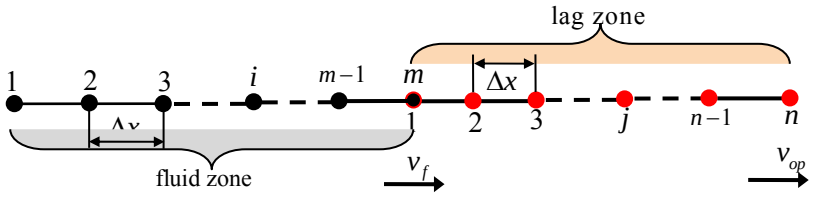

(a). Uniform moving mesh in the first stage.

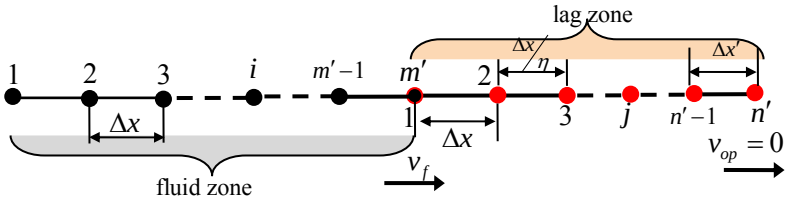

(b). Uniform moving mesh of the fluid zone and scaled down mesh of lag-zone in the second stage.

Fig. 2 Meshing strategy in the two stages

In the second stage the length of lag-zone becomes smaller and smaller owing to forward motion of fluid front, and the stress intensity factor K_I is needed to calculate for determining the start time of fracture propagation. In order to calculate K_I more accurately by the formula [19, 20]

$$K_I = 2\sqrt{\frac{l_{op}}{\pi}}\left[\int_0^{l_f}\frac{p(x,t)}{\sqrt{{l_{op}}^2-x^2}}dx+\int_{l_f}^{l_{op}}\frac{p'(x,t)}{\sqrt{{l_{op}}^2-x^2}}dx\right], \tag{11}$$

we need to re-mesh the lag-zone (mesh in fluid-zone is unchanged): mesh sizes in lag-zone are scaled down in proportion η ($\eta>1$) from mesh size Δx to an appropriate size $\Delta x'$ with node number n', see Fig. 2(b). m' is the corresponding node number in fluid-zone at some moment t_k in the second stage. Owing to $v_f \neq 0$ and $v_{op}=0$, the value of m' will increase and the value of n' will decrease as the fluid front moves forward. The proportion η is easily obtained by the first mesh size Δx, the last mesh size $\Delta x'$ and the initial node number N of re-meshed lag-zone:

$$\eta = \left(\frac{\Delta x}{\Delta x'}\right)^{1/N-1}. \tag{12}$$

The reason for re-meshing the lag-zone is that the second integral term of equation (11) at fracture tip ($x=l_{op}$) is singular, the smaller mesh size near the fracture tip is, the higher accuracy of K_I is achieved.

3.2 Discretization of lubrication equation and boundary conditions

About numerical discretization of lubrication equation (4) there are many different methods: integral scheme in FEM [6], central difference scheme in FVM [10], differential polynomial scheme in [16] and so on. In this paper we make use of a central difference format to discretize equation (4) for all points x_i ($i=2,3,\cdots,m-1$) in fluid-zone except the first and last nodes, which are described by the boundary conditions (5) and (6), (7),

$$\frac{w_{i,k+1}-w_{i,k}}{\Delta t}=\frac{3{w_{i,k+1}}^2}{12\mu}\frac{w_{i+1,k+1}-w_{i-1,k+1}}{2\Delta x}\frac{p_{i+1,k+1}-p_{i-1,k+1}}{2\Delta x}+\frac{{w_{i,k+1}}^3}{12\mu}\frac{p_{i+1,k+1}-2p_{i,k+1}+p_{i-1,k+1}}{(\Delta x)^2}, \tag{13}$$

where the subscripts i and k ($k=1,2,3\cdots$) denote node number and time step number, respectively. Δt is the time step. In order to avoid solving the nonlinear system of w, we regard the net pressure p as an unknown and w as a known, equation (13) can be rewritten as

$$\Delta t\left[\frac{{w_{i,k+1}}^2(w_{i+1,k+1}-w_{i-1,k+1})}{16\mu(\Delta x)^2}+\frac{{w_{i,k+1}}^3}{12\mu(\Delta x)^2}\right]p_{i+1,k+1}+\Delta t\left[-\frac{{w_{i,k+1}}^2(w_{i+1,k+1}-w_{i-1,k+1})}{16\mu(\Delta x)^2}+\frac{{w_{i,k+1}}^3}{12\mu(\Delta x)^2}\right]p_{i-1,k+1}-\Delta t\frac{{w_{i,k+1}}^3}{6\mu(\Delta x)^2}p_{i,k+1}=w_{i,k+1}-w_{i,k}, \tag{14}$$

which can be written in a matrix form,

$$\mathbf{Ap}=\mathbf{b}, \tag{15}$$

where $\mathbf{A}$ is a coefficient matrix with size $(m-2)\times m$, in each row of which only three non-zero elements. $\mathbf{p}$ is the unknown vector of fluid net pressure, $\mathbf{b}$ is a vector of the fracture node opening increment. The boundary condition (5) at the injection point is discretized as

$$\frac{w_{1,k}^3}{12\mu}\frac{p_{1,k}-p_{2,k}}{\Delta x}-\frac{Q_0}{2}=0. \tag{16}$$

The boundary conditions (6) and (7) at the fluid front is easy formulated

$$p_{m,k}=-\sigma_0. \tag{17}$$

Finally, adding the two discrete equations into system (15), a well-posed nonhomogeneous system with size $m\times m$ is obtained, which has a unique solution with the reversible matrix $\mathbf{A}$.

The boundary condition (8) is transformed into discrete form

$$\frac{w_{m+n-2,k}-w_{m+n-1,k}}{\Delta x}<\varepsilon_1, \tag{18}$$

where ε_1 is a very small quantity, denotes the calculation tolerance. Because in actual numerical calculation condition (8) cannot be achieved, only can be rewritten in an approximate form like equation (18). The condition of zero fracture opening can be satisfied by itself. About calculation of the fluid volume in fracture, we can think of fluid filled in each mesh segment as a trapezoid, so the total fluid volume is the area sum of all trapezoids and condition (9) is discretized as follows

$$\frac{\Delta x}{2}\sum_{i=1}^{m-1}\left(w_{i,k}+w_{i+1,k}\right)=\frac{Q_0 t_k}{2}. \tag{19}$$

3.3 Discretization of elasticity equation

According to meshing strategy in section 3.1 the whole integral from 0 to l_{op} for fracture opening (1) can be discretized in the sum of piecewise integrals in each mesh segment. The net pressure in each segment can be seen as a uniform distribution as a result of its small length. It means that the net pressure inside the integral symbol can be put out as follows

$$\frac{E\pi}{4\left(1-\nu^2\right)}w\left(x_I\right)=\sum_{i=1}^{m-1}\frac{p_{x_i}+p_{x_{i+1}}}{2}\int_{x_i}^{x_{i+1}}G\left(x_I,\zeta\right)d\zeta-\sigma_0\sum_{j=1}^{n-1}\int_{x_j}^{x_{j+1}}G\left(x_I,\zeta\right)d\zeta, \tag{20}$$

where subscript $I=1,2,\cdots,m+n-1$, denotes node number of the opened fracture. In the lag-zone net pressure is a constant.

4 Iterative algorithm

Governing equations (1) and (4) are complexly coupled each other within net pressure $p(x,t)$ and fracture opening $w(x,t)$, so the elimination method is not available here, numerical solution of this model can be obtained only by iteration convergence.

4.1 Solution of initial condition

The initial condition is already given by equation (10), in which only the initial length of fluid-zone l_f^0 is assumed known, the initial inlet pressure P_0 and the initial length of opened fracture l_{op}^0 are unknowns. Firstly, we give an estimate of inlet pressure, note as P_0^*. Substituting condition $w=0$ at $x=l_{op}^0$ and equation (10) with the known P_0^* into equation (20) yields

$$\sum_{i=1}^{m-1}\frac{p_{x_i}+p_{x_{i+1}}}{2}\int_{x_i}^{x_{i+1}}G\left(l_{op}^0,\zeta\right)d\zeta=\sigma_0\sum_{j=1}^{n-1}\int_{x_j}^{x_{j+1}}G\left(l_{op}^0,\zeta\right)d\zeta. \tag{21}$$

The relationship between node numbers m of fluid-zone and n of lag-zone can be estimated by using average estimates of integrals in two sides of equation (21),

$$\frac{P_0^*-\sigma_0}{l_f^0}(m-1)F_f=\sigma_0(n-1)F_l, \tag{22}$$

where F_f and F_l are average estimates of the left and right integrals in equation (21), respectively. The purpose of doing this is to obtain a relatively accurate estimate of l_{op}^0 for reducing iteration number and saving computing time. Secondly, substitute the two estimates P_0^*, $l_{op}^{0\,*}$ into boundary conditions (16) and (18), and iterate P_0^*, $l_{op}^{0\,*}$ until they meet conditions (16) and (18). At last, the relative initial time t_0 is solved by substituting the initial fracture opening $w_{i,0}$ into equation (19).

4.2 Global iteration

The acquisition of the complete initial conditions ($w_{i,0}$, $p_{i,0}$, l_f^0, l_{op}^0) means that model solution ($p_{i,k-1}$, $w_{i,k-1}$, l_f^{k-1}, l_{op}^{k-1}, $k=1,2,3\cdots$) at the previous time step t_{k-1} is known. Firstly, giving the estimate of l_f^k and then the estimate of $w_{i,k}$ at the current time step t_k, denoted as l_f^{k*} and $w_{i,k}^*$, the corresponding net pressure $p_{i,k}^*$ in fluid-zone can be obtained by system (15) with equations (16) and (17). Secondly, making use of $p_{i,k}^*$ and equations (21) and (22), the relatively accurate estimate of l_{op}^k can be obtained, denoted as l_{op}^*. Thirdly, combining estimates $p_{i,k}^*$ and l_{op}^* to compose the entire net pressure through the opened fracture, which will be substituted into elasticity equation (20) to obtain a new fracture opening $w_{i,k}^{**}$, the corresponding net pressure $p_{i,k}^{**}$ and the length of the opened fracture l_{op}^{**}, which are needed to satisfy the boundary condition (18) by iterating l_{op}^*. Finally, if the estimate $w_{i,k}^*$ and the new obtained $w_{i,k}^{**}$ satisfy the following relationship,

$$\sqrt{\sum_{i=1}^{m}\left(w_{i,k}^{**}-w_{i,k}^{*}\right)^2}<\varepsilon_2, \tag{23}$$

where ε_2 has the same meaning as ε_1, it means that $w_{i,k}^{**}$ and the corresponding $p_{i,k}^{**}$ meet the coupled system (1) and (4) for the given estimate l_f^{k*}. In addition, if $w_{i,k}^{**}$ and $p_{i,k}^{**}$ is the real solution of the model at the current time step, the condition (19) of

volume conservation needs to be satisfied. If it is not satisfied, iterating the estimates l_f^{k*}, $w_{i,k}^*$ and l_{op}^* to the above loops until they satisfy the two governing equations (15), (20), and the all boundary conditions (16), (17) (18) and (19).

4.3 Improvement of iteration method

It can be seen that in the global iteration algorithm there are 3 loop iterations: iteration of solution l_{op}^k corresponds to condition (18), iteration of solution $w_{i,k}$ corresponds to condition (23) and iteration of solution l_f^k corresponding to condition (19). It means that the estimates of l_{op}^k, $w_{i,k}$ and l_f^k determine calculation time and iteration number. If the estimates are closer to the accurate solution, it will waste less time and fewer iteration number by using appropriate iteration direction. The relative accurate estimate of l_{op}^k is given by equations (21) and (22).

The estimate of $w_{i,k}$ closer to the accurate we can obtain by fluid volume conservation. The fluid volumes at the previous and current time steps are written as

$$V_{k-1}=\int_0^{l_f^{k-1}} w(x,t_{k-1})dx,\quad V_k=\int_0^{l_f^k} w(x,t_k)dx. \tag{24}$$

It is known that fracture opening of plain-strain hydraulic fracture has self-similarity [23], so we assume that fracture openings at time steps t_{k-1} and t_k satisfy the following relationship,

$$w\left(x,t_k\right)=w\left(x\frac{l_f^{k-1}}{l_f^k},t_{k-1}\right)M_k,\quad 0\le x\le l_f^k \tag{25}$$

where M_k is a constant, has the meaning of average proportional coefficient about fracture openings. Substituting equation (25) into equation (24) and by variable substitution

$$V_k==M_k\frac{l_f^k}{l_f^{k-1}}V_{k-1}, \tag{26}$$

The two fluid volumes can also be obtained by inlet injection rate

$$V_{k-1}=\frac{Q_0}{2}t_{k-1},\quad V_k=\frac{Q_0}{2}t_k. \tag{27}$$

Combining equations (26) and (27), the constant M_k is obtained,

$$M_k=\frac{t_k l_f^{k-1}}{t_{k-1}l_f^k}>1, \tag{28}$$

where M_k being greater than 1 means that fracture opening at current time on the whole is greater than fracture opening at previous time for every nodes.

The estimate of l_f^k closer to the accurate can be obtained by the transient velocity of fluid front instead of average velocity at the interval Δt, which is described by lubrication theory [1],

$$v_f=-\frac{w^2}{12\mu}\frac{dp}{dx},\quad x=l_f \tag{29}$$

which is written in discrete form

$$l_f^{k*}=l_f^{k-1}+\frac{w_{m,k-1}^{\ 2}}{12\mu}\frac{p_{m-1,k-1}-p_{m,k-1}}{\Delta x}\Delta t. \tag{30}$$

Actually, l_f^{k*} is little larger than the real value because the transient velocity at t_{k-1} is greater than the average at interval $\left[t_{k-1},t_k\right]$.

4.4 Strategy of iteration direction

In order to accelerate convergence, for iteration direction of l_{op}^k and l_f^k we choose the interpolation search with time complexity O($\log(\log n)$) better than O(n) or O($\log n$) of the traditional sequential search or binary search [24]. For iteration direction of $w_{i,k}$ we choose the method of weighted mean, the detailed process is as follows: at the first iteration the estimate $w_{i,k}^1$ is used to get the new fracture opening $w_{i,k}^{1,1}$ by equations (15) and (20) (see section 4.2), and the error is calculated

$$\mathrm{E}_1=\sqrt{\sum_{i=1}^{m}\left(w_{i,k}^{1,1}-w_{i,k}^1\right)^2}, \tag{31}$$

If $\mathrm{E}_1<\varepsilon_2$, iteration stops, else $w_{i,k}^2=(w_{i,k}^1+w_{i,k}^{1,1})/2$ as the new estimate of the second iteration is substituted into the governing equations (15) and (20) for obtaining the new fracture opening $w_{i,k}^{2,2}$ and the second new error E_2. If $\mathrm{E}_2<\varepsilon_2$, iteration stops, else from the third iteration the new estimate $w_{i,k}^j$ is obtained by weighted mean of the two iterative average values $\left(w_{i,k}^{j-2}+w_{i,k}^{j-2,j-2}\right)/2$ and $\left(w_{i,k}^{j-1}+w_{i,k}^{j-1,j-1}\right)/2$ in the previous two iterations with the weights of reciprocal of their corresponding errors

$$w_{i,k}^{j}=\frac{\mathrm{E}_{j-1}\left(w_{i,k}^{j-2}+w_{i,k}^{j-2,j-2}\right)+\mathrm{E}_{j-2}\left(w_{i,k}^{j-1}+w_{i,k}^{j-1,j-1}\right)}{2\left(\mathrm{E}_{j-1}+\mathrm{E}_{j-2}\right)}, \tag{32}$$

where $j\geq 3$, it means that from the third iteration the iterating direction is slightly adjusted to quickly find accurate solution.

This strategy is able to guarantee that the estimate with smaller error contributes more to the new estimate for the next iteration, which makes the difference between the estimate $w_{i,k}^{j}$ and the new fracture opening $w_{i,k}^{jj}$ going to smaller and smaller in general as the iteration continues until convergence is achieved.

4.5 Determination of initial time scale

One important advantage of this model is that in solution of the initial conditions (section 4.1) a quantity of time scale, namely, the relative initial time t_0 is obtained according to fluid volume conservation

$$t_0=\frac{2V_0}{Q_0}=\frac{2}{Q_0}\int_0^{l_f^0} w_0(x)dx, \tag{33}$$

where V_0 is fluid volume at the time t_0, and $w_0(x)$ is the corresponding fracture opening. So we can use the magnitude of t_0 as the initial time step Δt.

It is more important to notice that as the fluid injection continues, velocity of fluid front becomes smaller, the number of fluid advancing meshes at each time step Δt will decrease, maybe even less than one mesh at some moment, so a certain threshold for advancing mesh number is necessary to ensure calculation continuity.

5 Numerical results

The algorithm is implemented in MATLAB R2018a, in which there are a lot of ready-made mathematical functions, especially integral calculation and its grammar is simple. The disadvantage is that when mesh number is large, computing speed for piecewise integral calculation will be slow. Relevant calculation parameters: Young's modulus $E=30\,GPa$, Poisson's ratio $\nu=0.2$, inlet injection rate $Q_0=3\times10^{-4}\,m^2/s$, far-field stress $\sigma_0=1\,MPa$, initial fracture length $l_0=0.5\,m$, mesh size $\Delta x=1\times10^{-3}\,m$, tolerances $\varepsilon_1=1\times10^{-4}$, $\varepsilon_2=1\times10^{-7}$, toughness $K_{Ic}=0.5\,MPa\cdot m^{0.5}$ and fluid viscosity $\mu=1\times10^{-3}\,Pa\cdot s$. The initial fluid-zone length at the corresponding relative initial time t_0 (unknown) is given as $l_f^0=5\times10^{-3}\,m$, namely 5 grid lengths.

5.1 Initial conditions and scale of time step

As shown in section 4.1 the pressure distribution of fluid-zone (10) is composed by the estimate inlet pressure P_0^* with the known l_f^0, which are substituted into the boundary condition (18) to obtain the corresponding length of opened fracture $l_{op}^{0\,*}$. Moreover, P_0^* and $l_{op}^{0\,*}$ need to satisfy the boundary condition (16) at the wellbore by iterating P_0^*. Table 1 shows the results of all initial conditions under $l_f^0=5\times10^{-3}\,m$. So according to the obtained value of the relative initial time we can set the initial time step $\Delta t=2.5\times10^{-4}\,s$, which can guarantee that magnitude of initial time step is the same as initial magnitude of time in this model.

Table 1. All initial conditions under $l_f^0=5\times10^{-3}\,m$

l_f^0 (m)	t_0 (s)	l_{0op}(m)	P_0 (MPa)	V_0 (m^2)
5×10^{-3}	2.3×10^{-4}	23×10^{-3}	14.07	3.5×10^{-8}

5.2 Evolution results

The evolution of fluid pressure and fracture opening at the first stage from initial partial open $l_{op}^0=23\times10^{-3}\,m$ to complete open $l_{op}=500\times10^{-3}\,m$ is presented in Fig. 3 and 4. From the two figures it can be seen that evolution of preexisting fracture open has the self-similarity as the evolution of fracture propagation [23]. In Fig. 3 we find that as fluid front moves forward, fluid pressure distribution become closer and closer to uniform. In Fig. 4 each curve of fracture opening is composed of two different lines: solid line and dotted line, which represent fluid-zone and lag-zone, respectively. The last curve is the contour of fracture opening when the preexisting fracture is opened completely, in which the ratio of fluid-zone and lag-zone agrees with the result in paper [25] when the fracture toughness is zero.

Figs. 5 and 6 show the evolution of fluid pressure and fracture opening from the first stage to the second stage. In the two figures the first curve

(t=0.123190) is the last one in the first stage (see Figs. 3 and 4), and the others are the distributions of fluid pressure and fracture opening in the second stage, in which length of opened fracture l_{op}=l_0 and fluid front keeps moving forward until fracture propagation condition $K_I = K_{Ic}$ is satisfied. From Fig. 6 it can be seen that fracture surface contour at the fracture tip changes from smooth tangent surface (t=0.123190) to arc surface (t=0.187296), which is due to existence of medium toughness ($K_{Ic} > 0$). This result is consistent with the experiment results [26]. This experiment study obtains that at the reopening phase the gradient of fracture width near the fracture tip is gradually decreasing to zero, but is increasing rapidly with the reducing distance to fracture front at the propagation phase.

Evolutions of inlet pressure and fluid front velocity in two stages are presented in Fig. 7, which suggests that at the initial injection the inlet pressure decreases rapidly on account of high fluid velocity, and as the injection continues, the fluid velocity becomes small, the inlet pressure decreases very slowly. It should be noted that because of mesh discreteness in numerical calculation there are stepped-decreases in evolution of fluid front velocity. In Fig.8 are illustrated evolutions about length of fluid-zone and length of opened fracture. This figure shows that in the first stage (left part of the vertical dotted line) the front of opened fracture moves faster than fluid front (slopes of the two curves), which leads to that length of lag-zone is increasing as injection continues, and at the end of the first stage velocity of fluid front is close to velocity of opened fracture front. When entering into the second stage (right part of the vertical dotted line, l_{op}=l_0), initial fracture is completely opened, fracture tip doesn't move forward until satisfying fracture propagation condition $K_I = K_{Ic}$, while velocity of fluid front continues to decrease.

Theoretically, because at the beginning the fracture is pre-existed, just closed, it means that there is no fracture toughness ($K_{Ic} = 0$) at the opened facture tip, so the stress intensity factor K_I at the first stage theoretically equals zero. The corresponding numerical results of stress intensity factor at the tip of opened fracture are showed in Fig. 9. The blue dots are the stress intensity factors in the first stage, the values are very close to zero, but not equal to zero of theoretical result. This is because that there are errors in calculating stress intensity as a result of singularity at the tip of opened fracture. the magnitude of errors about $10^3\ Pa \times m^{0.5}$ is very small compared with the magnitude of actual formation fracture toughness, which means that the algorithm accuracy is high. The second stage is the energy accumulation process, in which only fluid front moves, fracture front keeps still, which causes stress intensity factor to rise rapidly until equal to toughness (pink dots in Fig. 9).

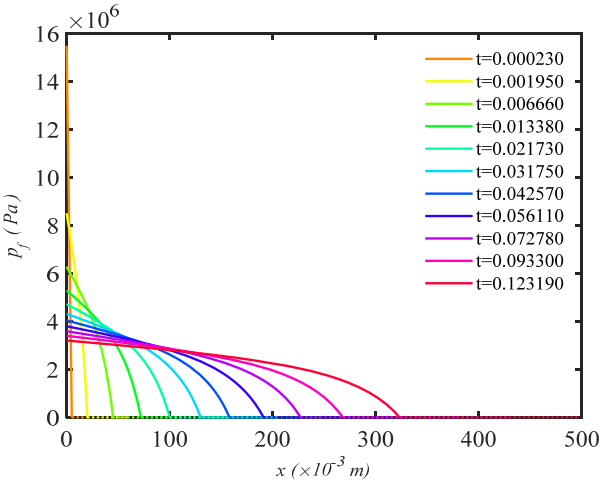

Fig. 3 Evolution of fluid pressure in the first stage.

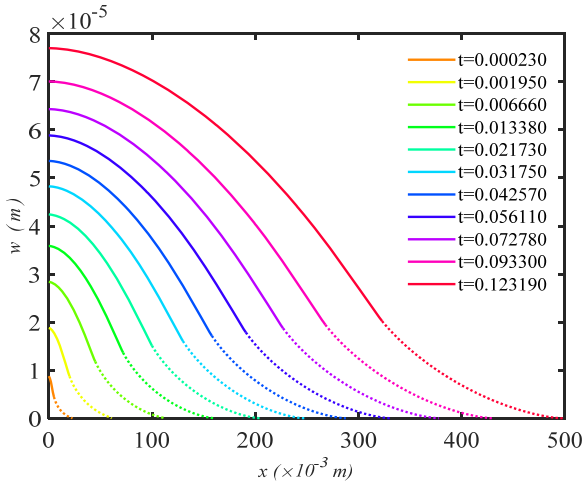

Fig. 4 Evolution of fracture opening in the first stage

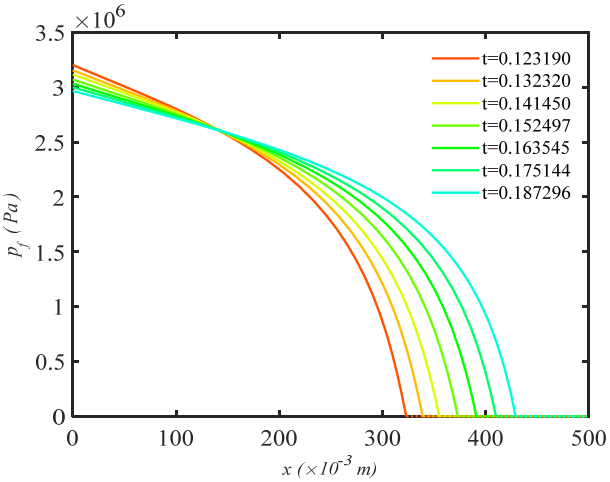

Fig. 5 Evolution of fluid pressure from the first stage to the second stage

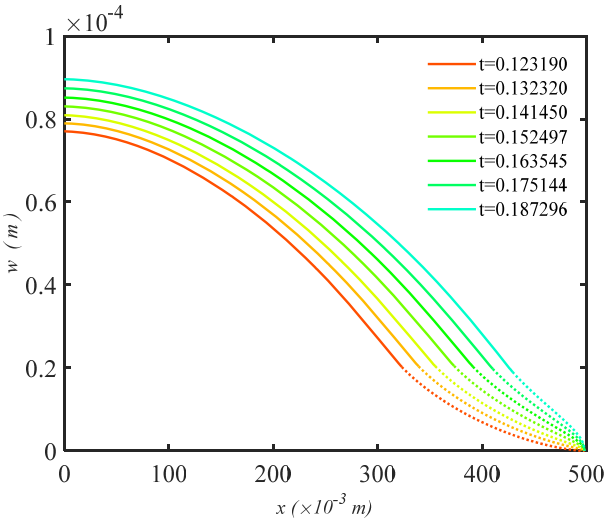

Fig. 6 Evolution of fracture opening from the first stage to the second stage

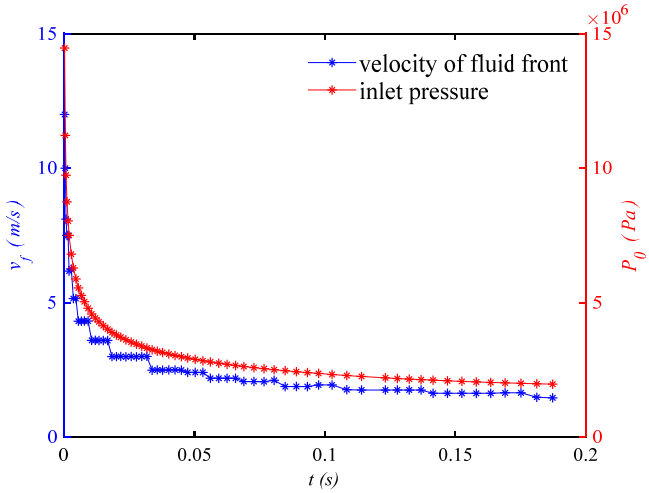

Fig. 7 Evolutions of inlet pressure and fluid front velocity in the two stages

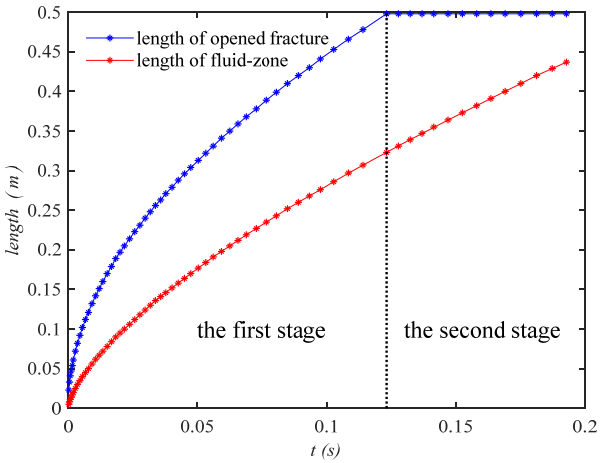

Fig. 8 Evolutions of length of fluid-zone and length of opened fracture

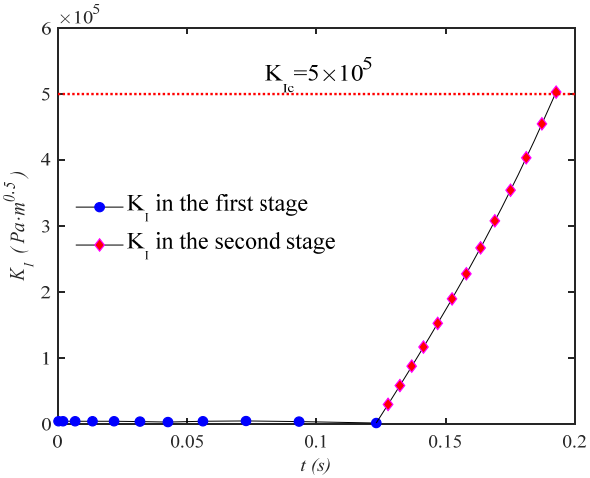

Fig. 9 Evolution of stress intensity factor at the tip of opened fractur

5.3 Analysis of algorithm

As analyzed in Section 4 at the first stage there are 3 unknowns l_f^k, l_{op}^k, w^k that need to be solved by iteration, at the second stage only 2 unknowns l_f^k, w^k remain to be determined. We have to estimate the values of these unknowns in advance due to the application of implicit algorithm for avoiding solving the nonlinear system. In Section 4 the detailed estimating methods for these unknowns are given, Figs. 10-13 show the corresponding results. Estimate and numerical values of lag-zone length at each time step are shown in Fig. 10, in which the estimates are obtained by equation (22), and the numerical values are convergence results. It can be seen that estimates are larger, but close to the numerical values on the whole, especially at the beginning.

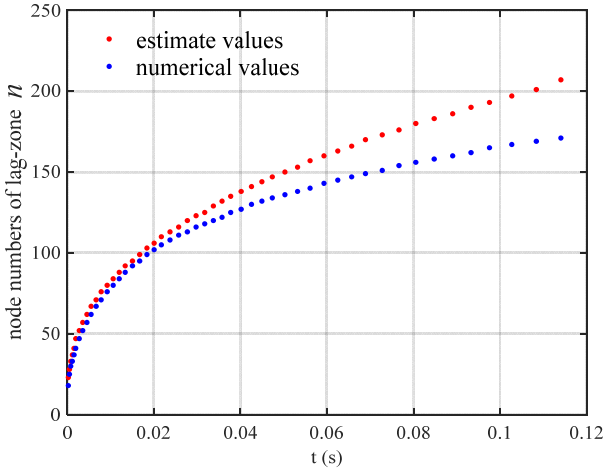

Fig. 10 Estimated and numerical node numbers n of lag-zone for each time step in the first stage

Fig. 11 compared the estimated and numerical values of proportional coefficient M_k. From this figure it can be seen that estimated values coincide very well with numerical values, which shows that estimates of fracture opening based on equation (28) is very close to numerical solutions. Also in Fig. 12 is given the result of estimated and numerical values of fluid front velocity at each time step, from which we can see that using the transient velocity of fluid front as an estimate of average velocity at period Δt is more reasonable and accurate. Fig. 13 shows the iteration numbers at each time step to verify the fast convergence of this improved iteration algorithm. From this figure we can see that iteration number exceeds 30 only 3 times, and the most iteration numbers are near 10 times, nearly a half are below 10 times. Our improved algorithm is faster than the numerical algorithm in the paper [17] with average 60 iteration times, which was widely used in many papers [13-16] for calculating the hydraulic problems.

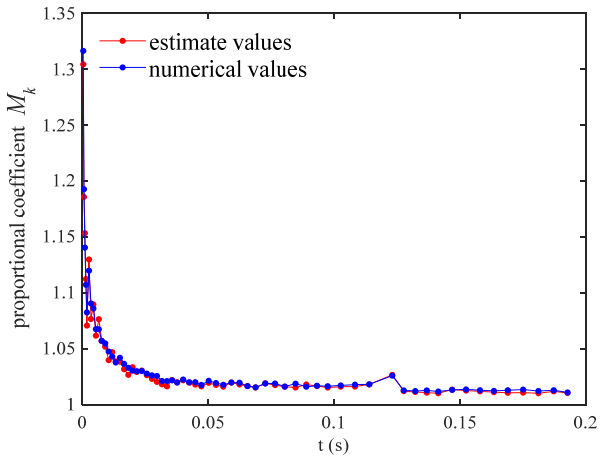

Fig. 11 Estimated and numerical values of M_k for each time step in two stages

According to fluid volume conservation (9) we analyse the accuracy of this algorithm. Fig. 14 gives the relative errors of fluid volume at each time step: the accurate fluid volume is obtained by $V_k = Q_0 t_k / 2$, the actual fluid volume V_k' is the volume enclosed by fracture contour in fluid-zone. And the relative error is calculated as

$$\xi_k = \left| V_k - V_k' \right| \Big/ V_k . \tag{34}$$

From this figure it can been seen that only at the beginning relative errors are little larger, but the largest error $\xi_k < 3.5\%$, most relative errors are less than 0.5%, which can verify that this improved algorithm have a high accuracy. From the above analysis, we can see that this implicit algorithm not only guarantees accuracy, but also greatly decreases iteration number and saves calculation time by utilizing accurate estimations of unknowns in the model.

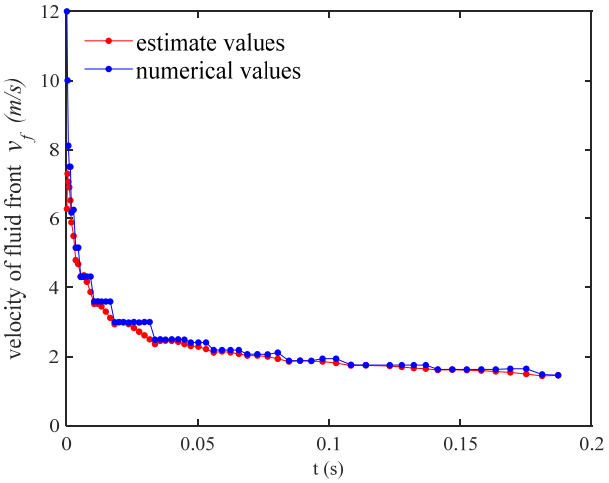

Fig. 12 Estimated and numerical values of v_f for each time step in two stages

5.3 Analysis of mesh length and time step

The average proportional coefficient M_k from equation (28) can be rewritten as

$$M_k = \frac{\left(t_{k-1}+\Delta t\right)\left(l_f^k - \Delta l_{k-1}\right)}{t_{k-1} l_f^k} = 1 + \frac{\Delta t}{l_f^k}\left(\frac{l_f^{k-1}}{t_{k-1}} - \frac{\Delta l_{k-1}}{\Delta t}\right), \tag{35}$$

Theoretically, M_k is greater than 1, so the following condition must be satisfied

$$\frac{l_f^{k-1}}{t_{k-1}} - \frac{\Delta l_{k-1}}{\Delta t} > 0. \tag{36}$$

The first and the second terms of inequality (36) have meanings of average velocity of fluid front at time intervals $[0, t_{k-1}]$ and $[t_{k-1}, t_k]$, respectively. This inequality is invariable, because transient velocity of fluid front is a monotonically decreasing function of time (see Fig. 12). It is known that l_f^k monotonically increases with time, the difference of the first and the second terms of inequality (36), noted as Δv_k, is a monotonically decreasing function of time, which is presented in Fig. 15. So it can be obtained from equation (35) that M_k is also a monotonically decreasing function of time under the condition of the constant Δt, namely $M_{k+1} < M_k$.

Although theoretically all M_k are greater than 1, actually at some moment certainly happens:

$M_{k+1}<1$ for numerical calculation, this is because at the previous time step M_k is very close to 1 and there is a calculation error owing to meshing discreteness. In order to avoid this case, we need to ensure that M_k is not too close to 1 in the whole calculation. In this paper a method of adaptive time step Δt_k when $M_k \to 1$ is applied to guarantee all $M_{k+1}>1$. Fig. 11 presents the evolution of M_k at every time step by using the adaptive time step method. From this figure it can be seen that the most values of M_k fluctuate around 1.02, the purpose of which is not only to ensure fast convergence but also to ensure calculation accuracy, because when Δt_k is larger, M_k will be much greater than 1 according to equation (35), convergence can be obtained rapidly, but calculation accuracy cannot be ensured; Otherwise, if Δt is smaller, M_k will be very close to 1, this means w_k is very close to w_{k-1} of previous time step, which will make it very difficult to converge. So in this model we use the condition

$$1.01 < M_k < 1.03 \tag{37}$$

as a balance of accuracy and convergence for this model. Need to point out that at the beginning M_k doesn't satisfy condition (38) because of large fluid velocity, and this condition is applied only to steady fluid flow when the velocity gradient of fluid front is small. Furthermore, this condition also affects scales of time step and mesh length, because at every time step moving length of fluid front must satisfy

$$\Delta l_k = v_f^k \cdot \Delta t \geq \Delta x, \tag{38}$$

where Δx is the grid length, satisfying condition (38) can ensure that at every time step fluid front can move forward not less than one grid length. In addition, v_f^k is decreasing with time (see Fig. 12), and Δx is constant (see Fig. 2), so the method of adaptive time step Δt_k is also needed to ensure that inequality (39) is always true. Evolution of time step with respect to calculating number k is presented in Fig. 16. It can be seen that Δt_k is gradually increasing with calculating number, except the two black dots. Need to point out that the first black dot is the critical point from the first stage to the second stage, at which needs to satisfy the condition of the opened fracture length equal to the initial fracture length ($l_{op}=l_0$), this is the reason why the time step increases sharply. And then after entering into the second stage time step returns to a reasonable value. The last black dot shows that time step decreases, this is because at that point need to satisfy the condition of fracture propagation ($K_I = K_{Ic}$) . Finally, the two combined inequalities (37) and (38) determinate time step and grid length for ensuring a fast convergence velocity and good accuracy.

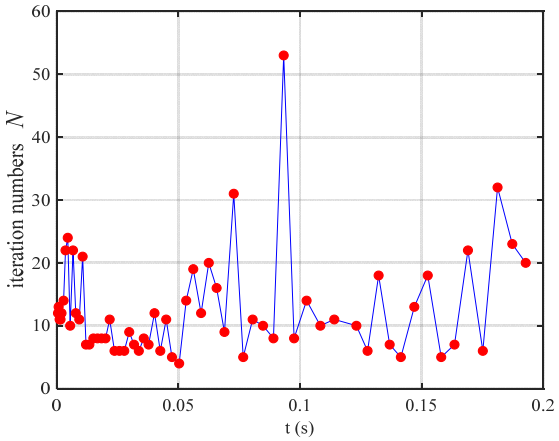

Fig. 13 Iteration numbers N_k for each time step in two stages

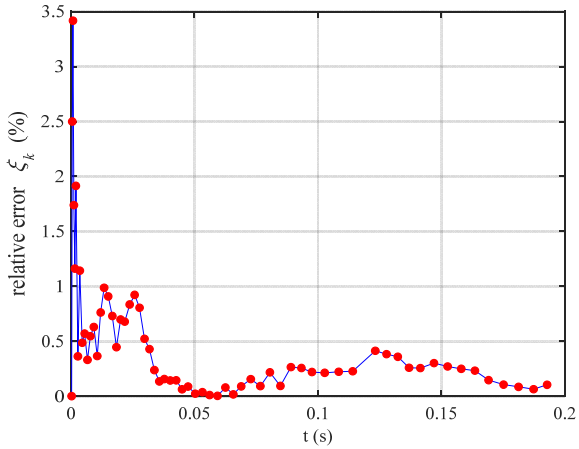

Fig. 14 Relative error ξ_k of fluid volume at each time step in two stages

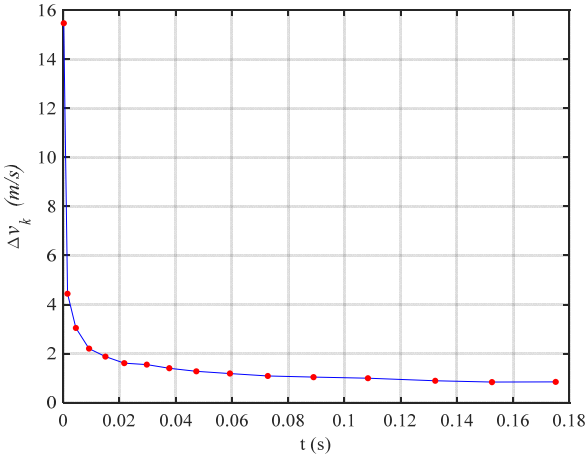

Fig. 15 Difference of two average velocities in inequality (36) with respect to time

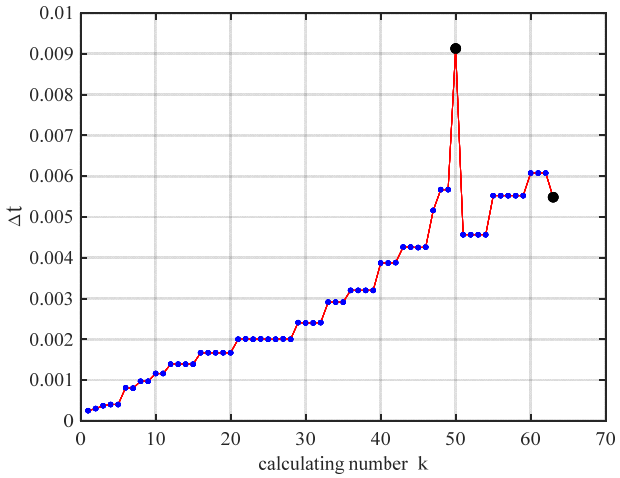

Fig. 16 Evolution of time step Δt with respect to the calculating number k

6 Conclusion

In this paper, we studied a new implicit algorithm to calculate the process from initial opening to initial propagation of a preexisting plain-strain hydraulic fracture with a fluid lag. In the algorithm an implicit difference scheme is adopted to avoid solving nonlinear equation system and the elasticity equation is transformed into the sum of piecewise integrals instead of the discrete polynomial expression to simplify calculation procedure, which is easily achieved in MATLAB R2018a. In this algorithm the relative accurate estimates of important unknowns: the length of fluid-zone l_f, the length of opened fracture l_{op} and fracture opening w at the next time step are obtained through transient velocity of fluid front, the condition of zero opening at the tip of opened fracture and the condition of fluid volume conservation, respectively; The weighted mean method with the weight of error's reciprocal is chosen as iteration direction. A fast convergence with an average 15 iterations per time step and the average error below 0.5% are obtained by this algorithm. In order to ensure the balance between convergence speed and calculation accuracy, a balance threshold ($1.01 < M_k < 1.03$) about scales of time step and grid length is put forward. The adaptive time step method is adopted in the whole calculation process to ensure that the average proportional coefficient M_k is within the balance threshold.

The overall numerical results show that self-similarity of fracture opening appears in the whole process. According to different boundary conditions at the front of opened fracture, the whole evolution is divided in two stages: the first stage from initial opening to full opening with the Barenblatt condition; the second stage from full opening to initial propagation with the fracture propagation condition being satisfied at the front of opened fracture, respectively. Different boundary conditions lead to different evolution characteristics of fracture opening especially near the fracture tip: at the first stage the opened fracture has a smooth closure, but upon entering into the second stage fracture contour at the tip becomes a blunt arc closure. At beginning fluid pressure distribution transforms very fast from steep straight type to elliptical type, then changes very slowly and approaches a quasi-uniform distribution as time goes on. In the whole evolution process stress intensity factor is equal to zero in the first stage because of preexisting-closed state of the fracture, and in the second stage stress intensity factor quasi-linearly and rapidly increases until reaching fracture toughness. The numerical results of stress intensity factor in the first stage also show that the calculation accuracy and the meshing strategy are reasonable.

Acknowledgements

Authors N.N.Smirnov and A.B.Kiselev in pursuing the present study were partially supported by the program of Russian Academy of Sciences "Development of algorithms and codes for multiscale processes and combustion simulations". AAAA-A18- 118041190145-1 (0065-2019-0021).
The study was launched by Russian Foundation of Basic Research, Project 16-29-15076, which terminated in 2018.

References:

[1] G.K. Batchelor, *An Introduction to Fluid Dynamics*, Cambridge University Press, 1967.
[2] I.N. Sneddon, M. Lowengrub, *Crack Problems in the Classical Theory of Elasticity*, John Wiley & Sons, 1969.
[3] G.R. Irvin, Analysis of stresses and strains near the end of a crack traversing a plate, *Journal of Applied Mechanics*, Vol.24, 1957, pp.361–364.
[4] G. I. Barenblatt, The mathematical theory of equilibrium cracks in brittle fracture, *Advances in Applied Mechanics*, Vol.7, 1962, pp.55-129.
[5] M. Wangen, Finite element modeling of hydraulic fracturing on a reservoir scale in 2D, *Journal of Petroleum Science and Engineering*, Vol.77, 2011, pp.274-285.
[6] M.J.Hunsweck, Y. Shen, A.J. Lew, A finite

element approach to the simulation of hydraculic fractures with lag, *International Journal for Numerical and Analytical Methods in Geomechanics*, Vol.37, No.9, 2012, pp.993-1015.

[7] M. Wangen, A 2D volume conservative numerical model of hydraulic fracturing, *Computers and Structures*, Vol.182, 2017, pp.448-458.

[8] B. Chen, S. Cen, A. R. Barron, D.R.J. Owen, C. Li, Numerical investigation of the fluid lag during hydraulic fracturing, *Engineering Computations*, Vol.35, No.5, 2018, pp.2050-2077.

[9] A. Lisjak, P. Kaifosh, L. He, B.S.A. Tatone, O.K. Mahabadi, G. Grasselli, A 2D, full-coupled, hydro-mechanical, FDEM formulation for modelling fracturing processes in discontinuous, porous rock masses, *Computers and Geotechnics*, Vol.81, 2017, pp.1-18.

[10] X. Chen, Y. Li, J. Zhao, W. Xu, D. Fu, Numerical investigation for simultaneous growth of hydraulic fractures in multiple horizontal wells, *Journal of Natural Gas Science and Engineering*, Vol.51, 2018, pp.44-52.

[11] L. Q. Choo, Z Zhao, H. Chen, Q. Tian, Hydraulic fracturing modeling using the discontinuous deformation analysis (DDA) method, *Computers and Geotechnics*, Vol.76, 2016, pp.12-22.

[12] L. Xie, K. B. Min, B. Shen, Simulation of hydraulic fracturing and its interactions with a pre-existing fracture using displacement discontinuity method, *Journal of Natural Gas Science and Engineering*, Vol.36, 2016, pp.1284-1294.

[13] D. Garagash, E. Detournay, The tip region of a fluid-driven fracture in an elastic medium, *Journal of Applied Mechanics*, Vol.67, 2000, pp.183-192.

[14] D. I. Garagash, E. Detournay, Plane-strain propagation of a fluid-driven fracture: small toughness solution, *Journal of Applied Mechanics*, Vol.72, No.6, 2005, pp.916-928.

[15] D. I. Garagash, Propagation of a plane-strain hydraulic fracture with a fluid lag: early-time solution, *International Journal of Solids and Structures*, Vol.43, 2006, pp.5811-5835.

[16] B. Lecampion, E. Detournay, An implicit algorithm for the propagation of a hydraulic fracture with a fluid lag, *Computer Methods in Applied Mechanics and Engineering*, Vol.196, 2007, pp.4863-4880.

[17] R. Carbonell, J. Desroches, E. Detournay, A comparison between a semi-analytical and a numerical solution of a two-dimensional hydraulic fracture, *International Journal of Solid and Structures*, Vol.36, 1999, pp.4869-4888.

[18] A. Pouya, V. L. Nguyen, S. Ghabezloo, Hydraulic fracture propagation under steady state flow, *The 48th US Rock Mechanics / Geomechanics Symposium*, Minneapolis, USA, 2014.

[19] J.R. Rice, *Mathematical analysis in the mechanics of fracture*, Vol.2, New York, NY: Academic Press. 1968, pp.191–311.

[20] J.R. Rice, Some remarks on elastic crack-tip stress fields, *International Journal of Solids and Structures*, Vol.8, No.6, 1972, pp.751–758.

[21] Y. P. Zheltov, S. A. Kristianovic, The hydraulic fracturing of an oil-producing formation, *Izvest. Akad. Nauk USSR, Otdel. Tekh. Nauk.* Vol.5, 1955, pp.3-41.

[22] J. Geertsma, F. de Klerk, A rapid method of predicting width and extend of hydraulically induced fractures, *Journal of Petroleum Technology*, Vol.21, No.12, 1969, pp.1571-1581.

[23] D. A. Spence, P. Sharp, Self-similar solutions for elastohydrodynamic cavity flow, *Proceedings of the Royal Society*, Vol.400, 1985, pp.289-313.

[24] Y. Perl, E. M. Reingold, Understanding the complexity of interpolation search, *Information Processing Letters*, Vol.6, 1977, pp.219-222.

[25] R. G. Jeffrey, D. Schlumberger, The combined effect of fluid lag and fracture toughness on hydraulic fracture propagation, *Low Permeability Reservoirs Symposium*, 6-8 March, Denver. 1989, pp.269-276.

[26] C. J. de Pater, J. Groenenboom, D. B. van Dam, R. Romijn, Active seismic monitoring of hydraulic fractures in laboratory experiments, *International Journal of Rock Mechanics & Mining Science*, Vol.38, 2001, pp.777-785.